Surface relief gratings manufactured by lithographic means being a candidate for VLT MOONS instrument's main dispersers

Harzendorf, Torsten, Michaelis, Dirk, Flügel-Paul, Thomas, Bianco, Andrea, Oliva, Ernesto, et al.

Torsten Harzendorf, Dirk Michaelis, Thomas Flügel-Paul, Andrea Bianco, Ernesto Oliva, Uwe Zeitner, "Surface relief gratings manufactured by lithographic means being a candidate for VLT MOONS instrument's main dispersers," Proc. SPIE 10706, Advances in Optical and Mechanical Technologies for Telescopes and Instrumentation III, 1070621 (6 September 2018); doi: 10.1117/12.2313164

SPIE.

Event: SPIE Astronomical Telescopes + Instrumentation, 2018, Austin, Texas, United States

Surface relief gratings manufactured by lithographic means being a candidate for VLT MOONS instrument's main dispersers

Torsten Harzendorf [*a], Dirk Michaelis [a], Thomas Flügel-Paul [a],
Andrea Bianco [b], Ernesto Oliva [c], Uwe Zeitner [a]

[a] Fraunhofer Institute for Applied Optics and Precision Engineering, Albert-Einstein-Strasse 7, D-07754 Jena (Germany); [b] INAF - Osservatorio di Brera, Brera 28, 20121 Milano (Italy)
[c] INAF - Osservatorio Astrofisico di Arcetri, Largo Enrico Fermi 5, I - 50125 Florence (Italy)

ABSTRACT

Surface relief gratings are well-established elements for high power laser applications, e.g. ultra-short pulse compression. A binary submicron period profile, realized by e-beam lithography and reactive ion beam etching in a dielectric material, is utilized for nearly one-hundred percent diffraction efficiency. Because these gratings are manufactured without any replication techniques, a high wave front accuracy and a low stray light background can be achieved. Spectroscopic applications require additional properties, i.e. a larger spectral bandwidth and Off-Littrow operation. We present new approaches for surface relief gratings realized either via multi-level staircase profiles or exploiting sub-wavelength features. The RVS spectrometer grating in ESA's GAIA mission is a prominent example where these techniques are already in use. The current contribution focuses on the results achieved during a pre-development performed for the MOONS instrument intended to operate at VLT.

Keywords: surface relief grating, electron beam lithography, multilevel, effective medium, spectrograph

1. INTRODUCTION

1.1 Binary surface relief gratings

A surface relief grating is a periodic structure with dimensions in the order of the wavelength of light engraved into the substrate surface. When light is propagating trough the micro-structured surface between two media with a different refractive index the phase of the light wave is altered and light will be diffracted. Only the period determines in which direction or orders the incident light of a certain wavelength and incident angle can be diffracted. The geometry within a period determines how the energy of light is distributed among the several orders. A binary grating is the simplest periodic arrangement of rectangular air grooves as shown in figure 1b.

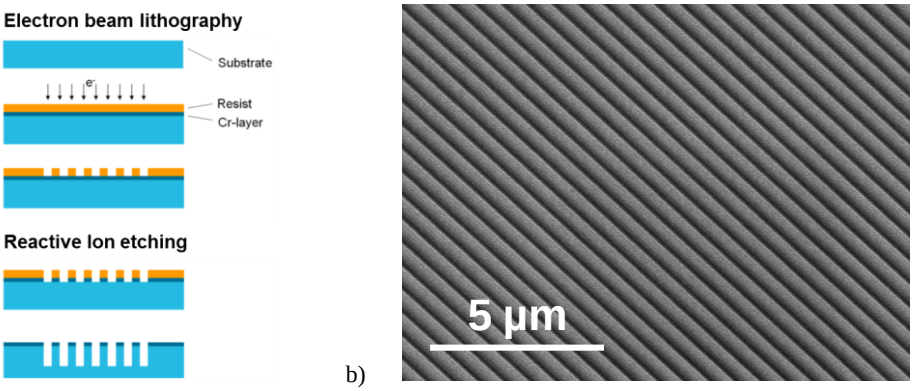

Figure 1. a) Fabrication process for binary surface relief gratings b) Scanning electron micrograph of a realized grating with 543 nanometers period (~1840 l/mm)

*torsten.harzendorf@iof.fraunhofer.de; microoptics.org

Advances in Optical and Mechanical Technologies for Telescopes and Instrumentation III, edited by Ramón Navarro, Roland Geyl, Proc. of SPIE Vol. 10706, 1070621 · © 2018 SPIE
CCC code: 0277-786X/18/$18 · doi: 10.1117/12.2313164

A binary grating profile is defined by the width and the depth of the groove in the substrate. These parameters can be changed to optimize the grating for the specific application. These gratings are well established in the field of ultra short pulse lasers, where nearly 100% of light in a single diffraction order can be achieved reducing the laser power losses while passing four times the grating for the pulse compression. For this purpose a grating with subwavelength period in Littrow configuration is used [1]. Such gratings are realized on the base of lithographic technologies like electron beam lithography and ion etching processes, which are adapted from semiconductor industries to optical applications. The fabrication process as shown in figure 1a starts with electron beam lithography. On the glass substrate a thin chromium layer is deposited. Then the resist, an electron beam sensitive material is spin coated. In the resist the grating lines will be written by electron beam lithography. To handle the writing time of such nanostructures a variable shaped electron beam writing tool SB350 OS of the company VISTEC is used. After the development of the resist the pattern is transferred by reactive ion etching into the chromium layer. The chromium layer then acts as a hard mask for the subsequent reactive ion etching step of the substrate material until the grating depth will be reached. Finally, the remaining chromium layer will be removed.

Due to the high process accuracy the gratings have a high performance with respect to wave front accuracy and stray light level, which makes the gratings well suitable for spectroscopic applications. Based on the described process a test grating for the Multi Object Optical and Near infrared Spectrograph MOONS [2] is realized. The grating operates in the YJ channel of the instrument with the following specifications summarized in table 1.

Grating type	Transmission
Period	2.045 µm
Polarization	TE and TM
Wavelength	910 – 1340 nm (channel YJ)
Angle of incidence	20 degrees (air)
Targeted diffraction efficiency in -1st order	> 70%
Target grating size	~ 300 mm in diameter

Table 1. Grating specification for the MOONS YJ channel

A binary grating profile is optimized with rigorous coupled wave analysis (RCWA) with the aim of a diffraction efficiency >70 percent over approximately 400nm bandwidth for both polarization states. The result is shown in Figure 2. The target efficiency is reached only in a limited bandwidth with a high polarization sensitivity.

The efficiency is so low because the period of the grating is larger than the operating wavelength and higher orders will occur, and the angle of incidence is set approximately 4 degrees out of Littrow condition for the center wavelength. In general, the specified bandwidth is too large for the binary grating approach.

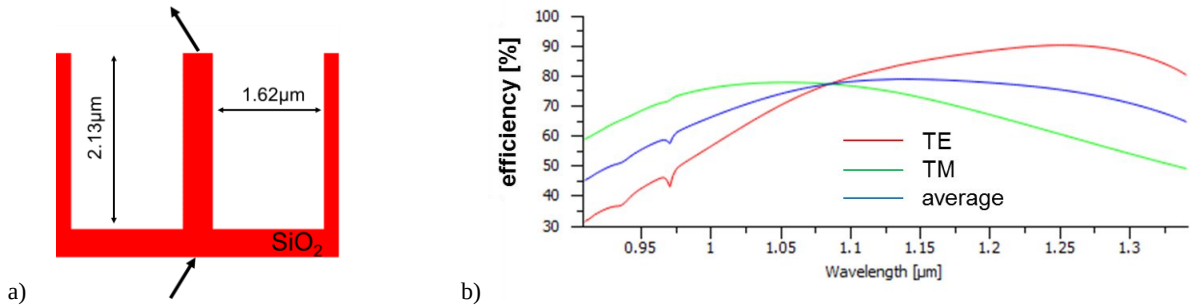

a) b)

Figure 2. a) Optimized binary grating profile and b) theoretical diffraction efficiency of the -1st diffraction order as a function of the wavelength as result of RCWA optimization for the MOONS YJ channel grating

1.2 More complex surface relief gratings

To overcome these limitations a transition to asymmetric grating profiles is needed. This can be realized by a blazed or sawtooth-like grating profile. By choosing the right blaze function, a single diffraction order will be preferred for the diffraction of light. For the realization of blazed profiles, other technologies are needed. Typically, analogue lithography, e.g. laser lithography or holography is used to generate continuous height profiles on the micrmeter scale. The challenge of these technologies is to keep the processes stable and reproducible to end up with the right grating profile. To be compatible to the standard binary lithographic techniques, the blazed profile is approximated by binary features. It can be done by either multilevel or staircase profile meaning grating grooves or ridges at different height levels. Alternatively, a 2D grating structure is utilized, where subwavelength features forming an effective medium, meaning an artificial refractive index profile within the grating period. This effective index structure then generates the blazed phase function (see Figure 3).

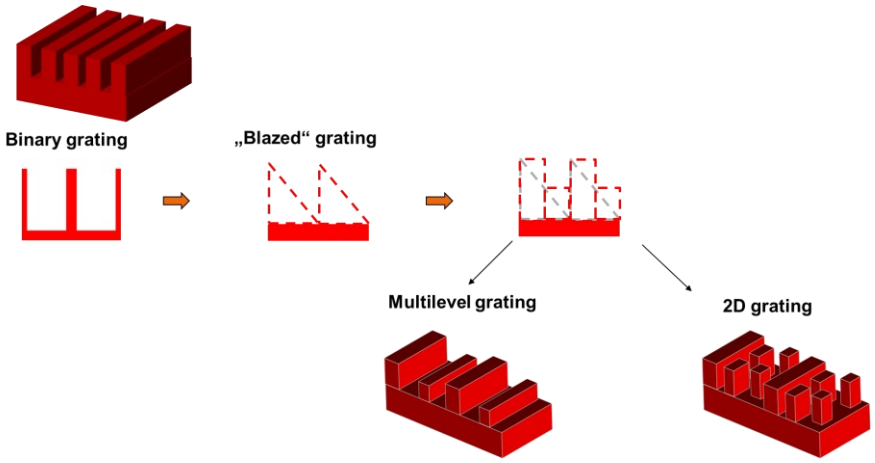

Figure 3. Transition from a binary surface relief grating to a more complex grating with a saw tooth surface profile, which is approached by binary features in either a multilevel grating with a staircase grating profile or a effective medium grating, in which two dimensional subwavelength features forming a blazed grating function by an artificial change of refractive index within the grating period

This approach is used already successfully for space spectroscopy in ESA's GAIA mission for the grating of the Radial Velocity Spectrometer. This was a transmission grating for the near infrared spectral imaging measuring the velocity of the stars in the Milky Way. The performance is outstanding in sense of diffraction efficiency >80% for both polarization directions and the small wave front error of less than 8nm root mean square on an area of approximately 200mm by 150mm, which is already large for electron beam lithography regarding the writing time by applying subwavelength features [3].

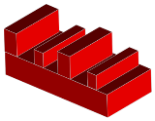

2. GRATING PROPOSAL I – MULTI LEVEL GRATING

2.1 Design

An additional grating ridge within the grating period gives the freedom in the design to adapt the operating point to an Off-Littrow configuration by breaking the symmetry of a binary grating. The grating profile is optimized by RCWA in the width and the position of the two grating ridges and also in their height. The resulting geometry is displayed in Fig. 4a. Figure 4b shows the theoretical diffraction efficiency in the -1st diffraction order of the grating. The goal of >70% averaged efficiency is reached almost over the full bandwidth of the spectral channel. Resonances become more prominent in the wavelength range, where the period is more than 2 times of lambda. The additional grating ridge is slightly decentered within the grating period and it seems that the position is related to the angle of incidence. A full theoretical explanation cannot be given at this moment. The optimization shows that the additional grating ridge must have a different height with respect to the first one to achieve this performance. That means 2 lithographic steps are necessary in the fabrication.

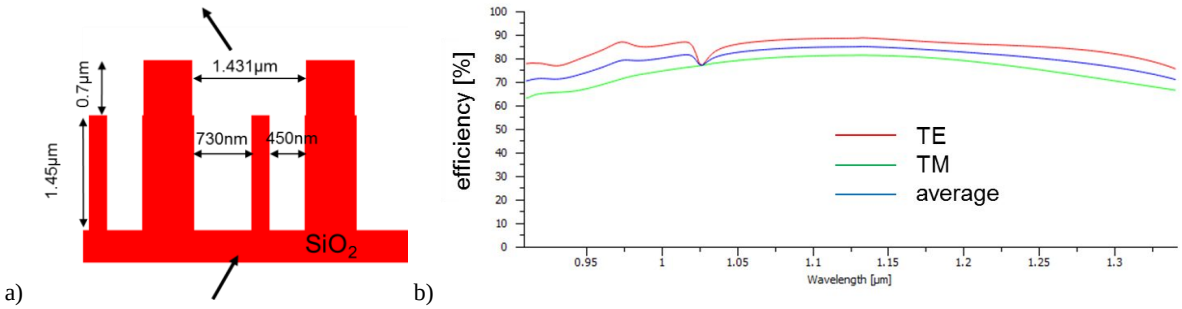

a) b)

Figure 4. a) Optimized multilevel grating profile and b) theoretical diffraction efficiency of the -1st diffraction order as a function of the wavelength as result of RCWA optimization for the MOONS YJ channel grating.

2.2 Technology

Multilevel technology is applied for the realization of this grating. Two sequential runs of electron beam lithography and reactive ion etching are performed, where the second lithography step is aligned to the first electron beam exposure. Tolerance analysis on the additional second grating ridge as shown in figure 5b illustrates that the tolerance on the position of this feature is more critical than deviations in width or height. Therefore, an alternative approach in the multilevel technology with relaxed alignment requirements is chosen (Figure 5a) [4].

The fabrication starts with the first electron beam lithography step. Test gratings of 20mm by 20mm size are placed on a 6 inch fused silica wafer (Figure 5b) varying the feature size of the two grating ridges by +/- 15nm to cover the fabrication tolerance of the lithographic process in lithographic exposure and chromium etching. Then the grating structure is etched into the fused silica substrate until the depth of level one is reached. The chromium mask is not removed at this moment. A second lithographic step is applied only with the purpose of removing the chromium mask partially from the second grating ridge, which can be done with relaxed alignment and accepting lateral sizing errors in lithography. The structure is etched in a second reactive ion etching step until the height of level 2 is reached. Finally, the chromium is removed from all grating features.

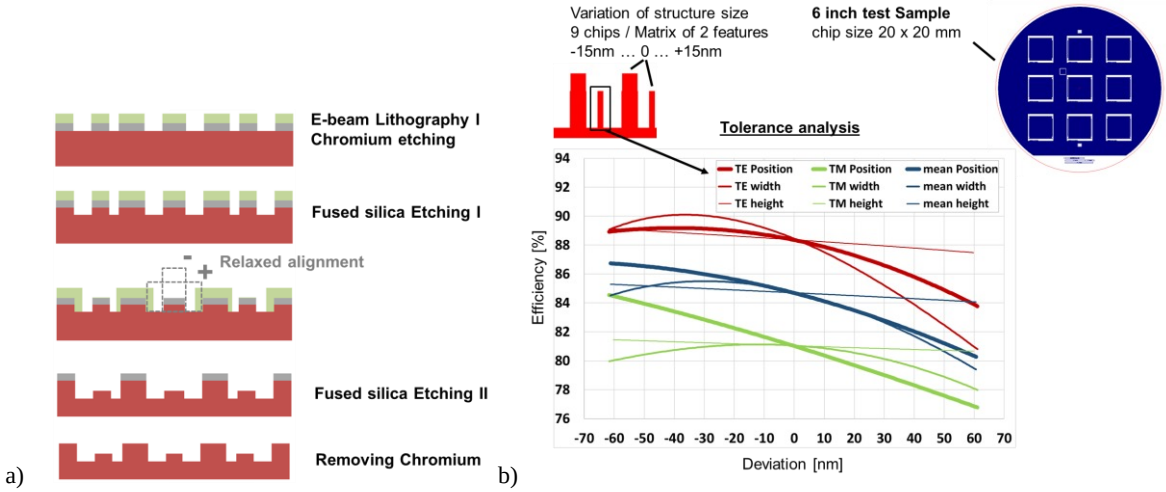

a) b)

Figure 5. a) Fabrication flow for the multi-level grating technology, b) Scheme of test sample and tolerance analysis

Fabrication results are shown in figure 6. The first scanning electron micrograph shows the lateral definition of all grating structures in the first lithography step. Consequently, no alignment or sizing error could be introduced by a second lithography step. The micrograph in the middle shows a cross section of the grating profile after the development of the resist in the second lithography step. It must be ensured that only the top of the small grating ridge is free to remove the chromium partially before the second deep etching step. The micrograph left shows the result after completing the fabrication. The deviations to the designed profile by certain effects are visible, e.g. trenching or lagging in the etching process.

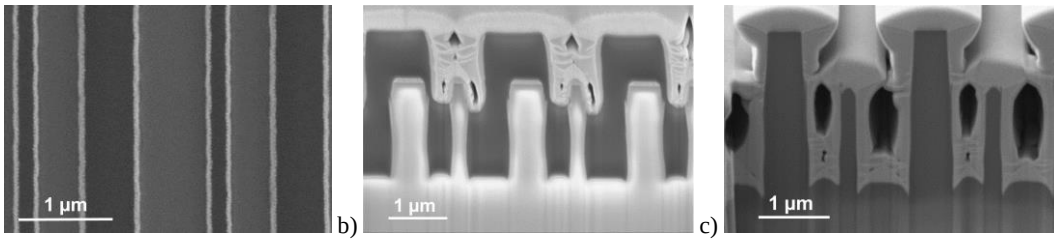

Figure 6. SE micrograph of a) chromium mask after first lithography b) cross-sectional view after second lithography c) cross-sectional view of the final grating profile. Cross sections are prepared by Focused Ion Beam.

2.3 Diffraction Efficiency Measurement

The grating performance is determined using an optical test bench, shown in figure 7. A fiber coupled laser source, which can be wavelength tuned, enables the measurement of diffraction efficiency at different wavelengths and both polarization stages. It is mounted on a goniometer arm to set the angle of incidence. A detector is mounted on a second goniometer arm to set the angle of diffraction. The grating test sample is scanned in two-dimensions to map the efficiency over the test grating matrix, also shown in figure 7. From the very homogenous distribution it can be concluded that the variation of feature size in the range of the fabrication tolerance do not influence the performance. Secondly, the map also shows that an existing inhomogeneity of the etching depth is very small and is also covered by a robust design. The measurement is done for 5 wavelengths distributed over the channel bandwidth.

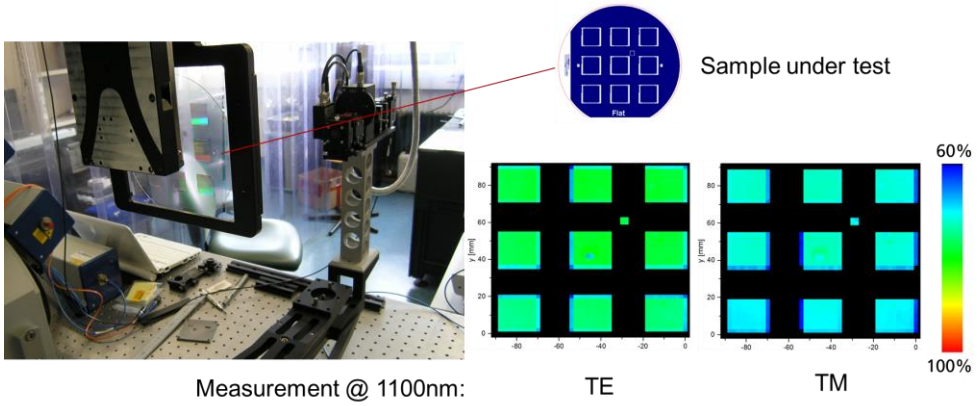

Figure 7. Diffraction measurement set-up and mapping result of the grating test sample

Because the sample was not AR-coated, the measurement values which are the average of the scanned grating area, are corrected by Fresnel losses and compared to the theoretical values (Figure 8b). The efficiency values are remarkably reduced at higher wavelengths. For analysis of deviations in the fabrication process, the realized grating profile is extracted from the cross sectional SEM image (Figure 8a) and recalculated in the grating design. The optical performance is slightly influenced in some details but the overall performance is on the same level as the initial design. In conclusion, the deviation in feature size or shape is less critical. It cannot explain the drop of efficiency.

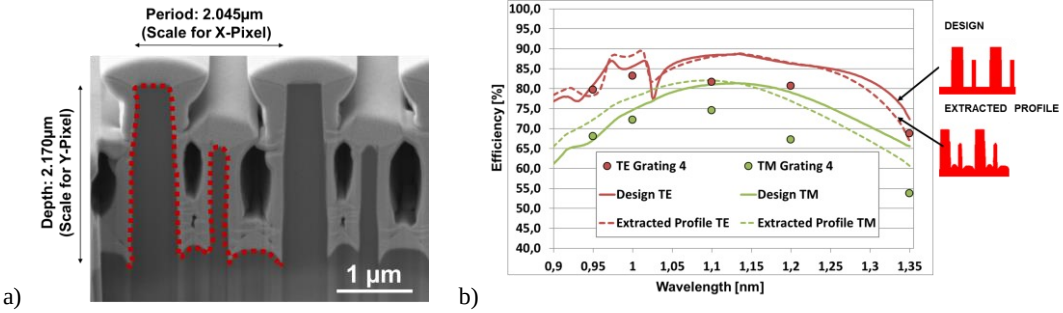

Figure 8. a) Profile extraction of the grating cross section for design analysis. b) Measured efficiency as a function of the wavelength and polarization compared to the theoretical values of the initial design and the analyzed profile

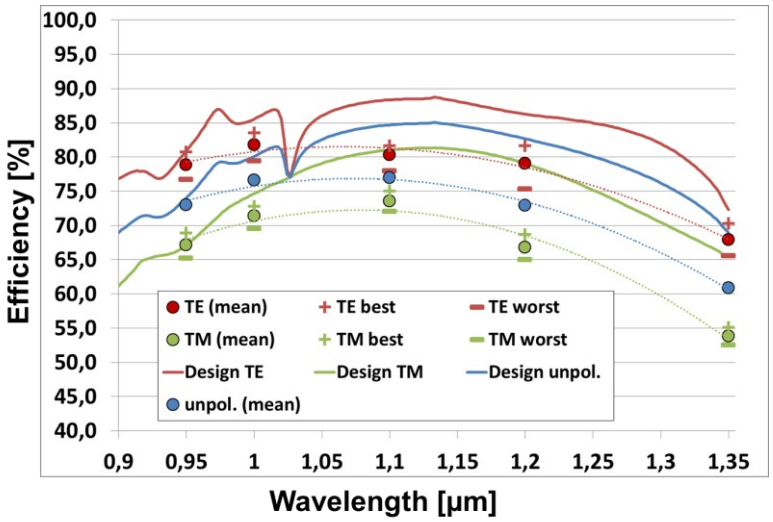

Figure 9. Measured efficiency as a function of the wavelength and polarization compared to the theoretical values of the initial design. Measurement values are corrected by Fresnel losses and shown for the mean value over all gratings and best and worst performing grating

However the measurement is done for all nine test gratings and shown as mean value of all gratings in figure 9. The efficiency goal is reached for nearly 3/4 of the spectral channel. The deviation from measurement to the design is not fully understood at this moment. The differences of the worst and best performing grating of each single measurement point are very small and show a minor influence of fabrication tolerances to the grating performance, indicating a robust grating design.

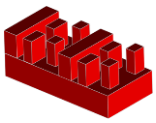

3. GRATING PROPOSAL II – EFFECTIVE MEDIUM GRATING

3.1 Design

The second grating structure is proposed according to the effective medium approach. Also here, subwavelength features are implemented having a periodic arrangement in the second dimension with a period at subwavelength scale so that the light will not be diffracted in the cross direction. In the effective medium approach the size and the position of the grating features determine the profile of a refractive index change from the substrate material to the air for the purpose of approaching a blazed function and this is also optimized by rigorous coupled wave analysis. The design result and the theoretical diffraction efficiency, which can be achieved for the MOONS YJ-channel grating is shown in figure 10a,b.

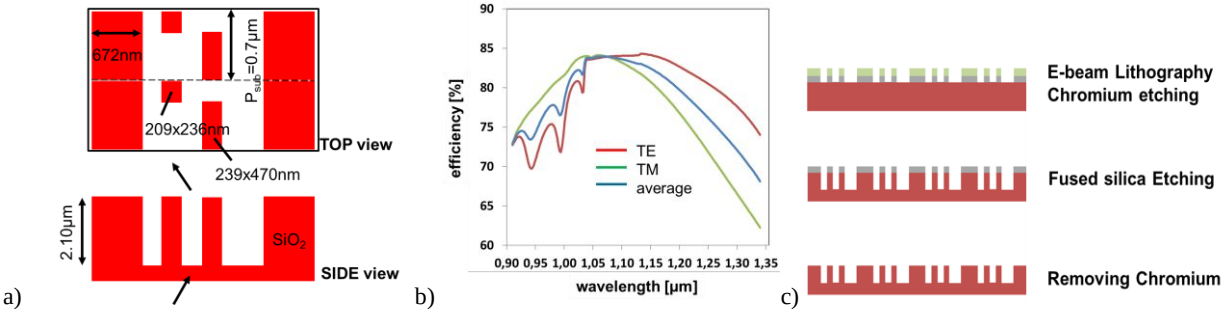

Figure 10. a) Design, b) theoretical diffraction efficiency, and c) fabrication flow for the 2D grating

3.2 Technology

An advantage of this design approach that the same structure height of all features so that the grating structure can be fabricated with a single lithographic run (figure 10c). A test wafer is fabricated by electron beam lithography, where a feature size variation of -10nm to +10nm is implemented into the test gratings. The result of this variation after electron beam lithography and chromium etching is shown in figure 11a. The technology is approaching the point where the small gaps between the grating ridges are not resolved due to the proximity effect in electron beam writing. Typically, this is corrected by complex mathematical algorithms locally adapting the electron dose. However, for such a complex arrangement of small features the algorithm fails. The structure is transferred by reactive ion etching into the fused silica substrate material. Pencil point like profiles are generated due to a faster chromium mask erosion for small two dimensional features (figure 11b). This effect is dependent from the initial structure size and can lead to the case that the chromium mask is completely consumed before the process end and the structure gets a smaller height (seen in cross section in figure 11c). The simulation is difficult because aside from the structure size the effect is influenced by the neighboring structures.

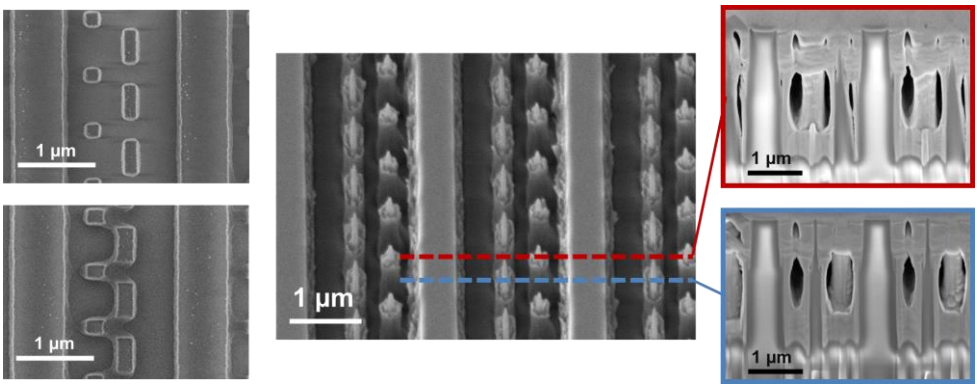

Figure 11. SE micrograph a) of grating structure after chromium etching by varying the nominal feature size by +/- 10nm b) after etching into the fused silica substrate, c) cross section of the grating at the indicated positions

3.3 Diffraction Efficiency Measurement Results

The diffraction efficiency measurement results are shown in figure 12. In general, the measurement values are in good correlation to the grating design. A huge variation of grating performance is identified by varying the feature size.

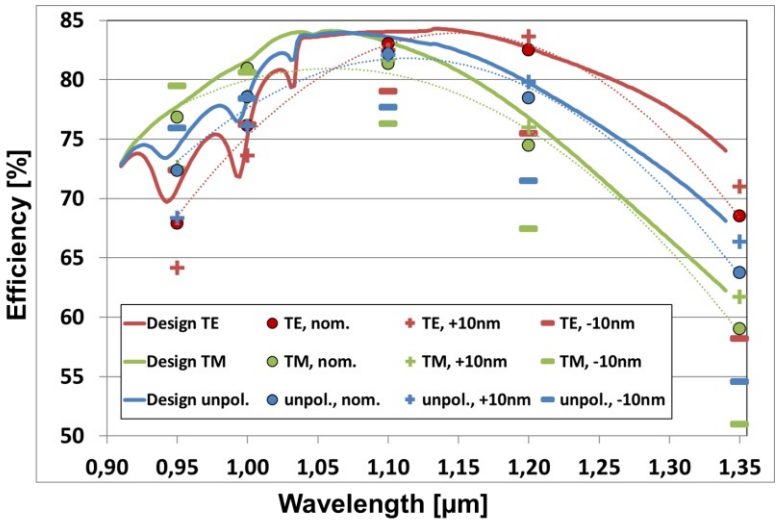

Figure 12. Measured efficiency as a function of the wavelength and polarization compared to the theoretical values of the initial design. Measurement values are corrected by Fresnel losses and shown for the gratings with feature size variation.

The deviation to lower efficiency values is more significant for the smaller features sizes, which are not resolved in the electron beam lithography as already shown in figure 11a. In the first run all features sizes are varied by the same amount in x- and y-direction. Reducing the feature size leads to a better performance at shorter wavelengths. Increasing the feature sizes give higher efficiency values at the longer wavelengths in the bandwidth of the channel. The overall performance can be improved by varying the feature size of each feature in x- and y-direction individually. The influence of changing the feature size onto the grating profile formation in the technological process cannot be foreseen with adequate accuracy to simulate the grating performance in advance. Therefore, a second technological run with a matrix of a higher number of test gratings on smaller grating size is proposed to optimize the lithographic layout taken all process effects into account. Nevertheless, the variation of feature size is in the range of the fabrication tolerance and is critical in the sense of reproducibility.

4. CONCLUSION & OUTLOOK

4.1 Comparison of two proposals

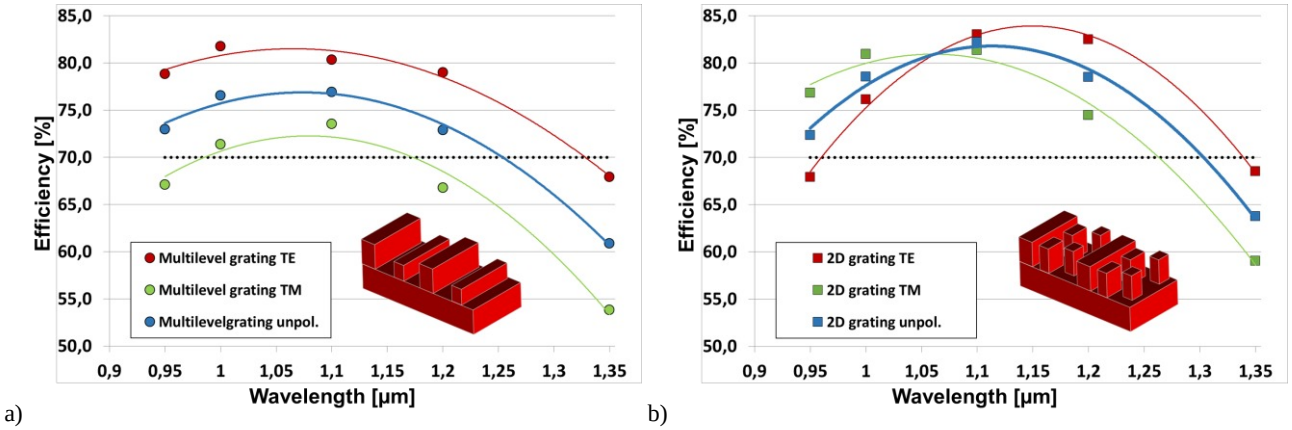

a) b)

Figure 13. Diffraction efficiency as a function of wavelength and polarization a) for the multilevel grating b) for the 2D grating

In summary, gratings which are aimed as dispersive element for the NIR channel of an astronomical spectrograph were fabricated by lithographic techniques according to two different approaches in design and technology, both having its own advantages and disadvantages. Both solutions are able to fulfill the efficiency requirement of >70% averaged in polarization which is nearly reached for the fabricated gratings (figure 13). The multilevel solution has a fabrication tolerant design. The one-dimensional grating lines have a small e-beam writing time. However, 2 lithographic steps are needed to get this high performance. The situation for the 2D grating is opposite: one has to realize an accuracy in feature size of about +/- 10nm after passing the complete lithographic processes with all of its influences on the feature size and feature profile, but only one lithographic step is needed. The writing time for a single electron beam lithographic exposure of the two-dimensional features will be more than a factor of 1.5 related to the 2 exposures of the multilevel grating. At the end a decision for one of these solutions will a balance of costs and process reliability, which could give a different picture for larger gratings.

4.2 Extension to larger grating areas

In general, both technologies can be extended to 300mm grating size by using electron beam lithography. It has to be tested how the inhomogeneity of the fabrication processes is affected by the enlarged area and how the grating performance will be influenced. For the test of the multilevel grating the first electron beam lithography step is performed in more than 30h exposure time. The performance is measured on a 300nm test structure in a 15mm x 15mm spaced matrix using a CD – Scanning electron microscope (figure 14). A feature size distribution of around 20nm over the whole wafer area would be sufficient for the multilevel approach and is already demanding for the 2D grating.

Another challenge of the 2D grating is the electron beam writing time, which is estimated with more than 4 days exposing the full 300mm sized wafer. The exposure time could be reduced by a shot count reduction of factor 9 utilizing the sophisticated cell projection writing regime in electron beam lithography [5].

a) 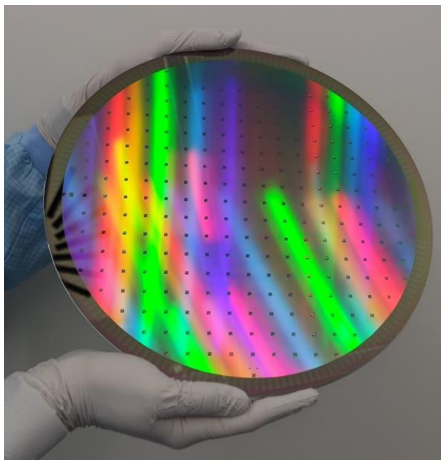 b)

303
301 301 303 303 301 303 306 302 296
301 304 305 306 310 311 309 312 308 306 306
302 303 305 307 308 306 310 310 311 313 311 309 309
297 302 303 307 307 309 307 310 312 310 309 314 310 314 309
299 303 306 305 307 304 309 310 310 311 314 312 313 313 314 315 309
302 302 306 309 307 310 309 310 313 313 317 316 316 314 315 315 310
303 307 307 306 309 308 309 307 314 312 313 316 315 317 318 315 315
302 304 309 308 311 309 308 309 309 311 317 318 314 317 317 316 316
302 305 306 309 308 308 312 310 312 316 314 314 315 317 313 317 315 315 310
304 305 308 305 314 313 313 312 315 311 316 316 317 316 313 314 314
305 306 308 312 310 308 311 313 312 313 318 315 317 315 314 315 309
302 304 307 306 312 310 312 306 308 312 312 313 316 314 313 313 305
298 303 307 307 308 307 309 309 311 311 310 313 313 314 316 307 306
300 303 304 306 308 308 311 310 312 312 309 312 314 312 309
300 304 304 305 308 310 309 306 312 309 309 308 307
303 301 306 304 305 308 308 311 305 304
299 299 301 301 304 304 304 303 302
302

Figure 14. First lithography test for the multilevel grating on a) a 300 millimeter wafer and b) related CD-SEM measurement result of a 300nm test structure in a 15mm x 15mm test matrix

REFERENCES

[1] Clausnitzer, T., Kämpfe, T., Kley, E.-B., Tünnermann, A., Tishchenko, A. V. and Parriaux, O., "Highly-dispersive dielectric transmission gratings with 100% diffraction efficiency," Optics Express Vol. 16 No. 8, 5577-5584 (2008).

[2] Cirasuolo, M., Afonso, J., Carollo, M., Flores, H., Maiolino, R., Oliva, E. et al, "MOONS: the Multi-Object Optical and Near-infrared Spectrograph for the VLT," Proc. of SPIE Vol. 9147, 91470N-1 (2014).

[3] Zeitner, U. D., Oliva, M., Fuchs, F., Michaelis, D., Benkenstein, T., Harzendorf, T., Kley, E.-B., "High performance diffraction gratings made by e-beam lithography," Appl Phys A (2012).

[4] Oliva, M., Harzendorf, T., Michaelis, D., Zeitner, U. D. and Tünnermann, A., "Multilevel blazed gratings in resonance domain: an alternative to the classical fabrication approach," Optics Express Vol .19 No. 15, 14737-14745 (2011).

[5] Kley, E.-B., Schmidt, H., Zeitner, U. D., Banasch, M. and Schnabel, B., "Enhanced e-beam pattern writing for nanooptics based on character projection," Proc. SPIE Vol. 8352, 83520M (2012).